Passive elastography of the esophagus: from model to preliminary in-vivo experiments using diameter measurements

Victor Delattre, Stefan Catheline, Gabrielle Laloy-Borgna, A Zorgani, S Roman

PASSIVE ELASTOGRAPHY OF THE ESOPHAGUS: FROM MODEL TO PRELIMINARY *IN-VIVO* EXPERIMENTS USING DIAMETER MEASUREMENTS

V. DELATTRE[1], S. CATHELINE[1], G. LALOY-BORGNA[1], A. ZORGANI[1], SABINE ROMAN[1,2]
[1]*INSERM U1032 LabTAU, Université de Lyon, Lyon, France*
[2]*Hospices Civils de Lyon, Hôpital Edouard Herriot, Lyon, F-69003, France*

E-mail: victor.delattre@inserm.fr

Abstract

Numerous diseases alter the esophagus elasticity, such as eosinophilic esophagitis and esophageal motility disorders like achalasia. The possibility to measure these modifications using minimally invasive techniques is a key issue for the diagnosis of such pathologies. The commercially available Endoflip™ (endoluminal functional lumen imaging probe) can be used to measure the luminal cross-sectional diameter of the esophagus at different points and over time, and is used in clinical routine to assess esophageal distensibility. We used this probe to track the propagation of shear waves similar to those that are produced naturally by physiological noise, to compute wavelength of the esophagus using passive elastography algorithms. What we mean by physiological noise is the natural vibrations of soft tissues caused by the heartbeat, muscle activity, arterial pulse wave etc… To assess the feasibility of such measurements, we compared the wavelengths obtained with the probe in vibrating polyvinyl alcohol gel tubes to those obtained for the same vibrating tubes with optical tracking of their edges using a high-speed camera. We first compared the wavelength obtained with homogeneous gel tubes with both techniques, and then used paired gel tubes of different elasticities to investigate the possibility to measure different wavelengths. Although, the wavelength computed using the probe and the high-speed camera showed some small differences, qualitative differentiation of the tubes was achieved when using paired tubes with different elasticities. Using the high-speed camera, a wavelength of 61 mm was measured for the hard tube, and 0.035 m for the soft tube. Using the probe, wavelengths of 61 mm and 38 mm were measured, respectively. Therefore, we demonstrate here the feasibility of using this probe to track wave propagation and to determine the wavelengths in gel tubes of different stiffnesses. This analysis was also taken to a preliminary *in-vivo* study that allowed tracking of natural waves in the esophagus using the luminal probe, which indicates that this technique can also be used *in vivo* to measure the stiffness of the esophagus.

Keywords: Elastography, Esophagus, Wave propagation

1.Introduction

Dysphagia is a common symptom that is characterized by a difficulty to swallow solids and/or liquids [1]. This might be related to esophageal motility disorders, which include loss of contractility and impaired relaxation of the esophago-gastric junction. These motility abnormalities can be secondary to inflammation and/or fibrosis of the esophageal wall. Esophageal impedance planimetry was recently developed using a commercially available endoluminal functional luminal probe, to evaluate esophageal distensibility in response to esophageal distension [2]. This probe consists of a catheter with 10 impedance rings and a pressure sensor, which are positioned within a balloon that is filled with saline solution. The balloon can be inserted into the esophagus, with step-wise distension achieved by filling the balloon with the saline solution. The diameter of the balloon is proportional to the impedance measured between the rings, and the distensibility of the esophagus can be estimated by dividing the diameter of the balloon by the pressure. The distensibility used by clinicians is closely linked to the elasticity of the esophagus. In the field of elastography, it is now well established that the wave speed allows estimation of the elasticity [3],[4]. Therefore, to estimate the wave speed as a proxy for the elasticity, we can measure the propagation of the natural waves along the esophagus caused by the beating of the heart. Such natural waves have already been used for the measurement of the viscoelastic properties of various tissues, such as liver [5], brain [6], and cornea [7] using ultrasoung imaging. Shear wave elastography can also be performed using other imaging modalities, such as MRI [8]-[10], OCT [11]-[13] and direct optical imaging [14] such as what we performed in this study. The temporal resolution of the luminal probe is not an issue when it comes to measuring wavelength. Indeed as we are correlating instantaneous spatial signals we are not subject to Shanon's criterion as explained in

[15]. It is also important to note here that the waves we are tracking are not due to the contraction of the esophagus, but are mechanical waves guided by the walls of the esophagus. They are due to all the physiological processes inducing movement in the human body, and their velocity and wavelength are linked to the wall stiffness.

The goal here is to show that the developed method is able to distinguish PVA tubes of different stiffnesses. This is performed by measuring the wavelength of elastic waves guided by the tube, being a PVA tube or an esophagus. The theory of waves guided by tubes has first been developed by Gazis [16],[17], investigating the different kind of modes that can propagate along a tube, as well as the evolution of their velocity with frequency, called dispersion. He showed that three types of modes can propagate along a tube, named L-, F- and T-modes, designating respectively axi-symmetric modes, called breathing modes, flexural modes and torsional modes. In this experiment, since we are looking at a 2D image of the tube, torsional modes cannot be observed. However, both breathing and flexural modes can be detected when using a high speed camera and detecting the edges of the tube. Since the in-vivo application consists in estimating the esophagus stiffness using the luminal probe which only measures the diameter of the esophagus, we are focusing only on waves that induce a local variation of the tube diameter. The guided modes that induce a local variation of the diameter are axisymmetric modes, also called breathing modes. Several breathing modes exist and they have different deformation profiles, but the first mode, named L(0,1) [18],[19] is the only mode without cutoff frequency. Hence it exists at all frequencies, including very low frequencies. This breathing mode L(0,1) is the guided mode corresponding to the pulse wave usually investigated in arteries [20],[21] Moreover, the study of guided waves in arteries has already been performed [22]-[24], and allows to access the arterial stiffness, giving an indicator of the cardiovascular health of a patient. At low frequency, the dispersion curve of the breathing mode is similar to the Lamb wave dispersion curve of a symmetric mode propagating along a plate [18],[19]. Hence the wave velocity at low frequency corresponds to the double of the Rayleigh wave velocity, being directly proportional to the square root of the shear modulus in biological tissues. Therefore, the velocity and so the wavelength of these axisymmetric guided waves along a tube gives at least qualitative information on the shear elasticity of walls of the tube.

Our preliminary studies here used gel tubes of different stiffnesses to mimic the esophagus, and the elastic waves were induced using mechanical vibrators. The elasticity was estimated using two independent wave-tracking devices: the luminal probe, and a high-speed camera.

Studies using vibrometry to measure porcine esophagi shear modulus have already been done [25] but here, the greatest innovation consists in the use of a probe that is already in clinical use to determine the elastic wavelength using noise correlation methods. Significant differences in the wavelengths between these soft and hard gel tubes were seen with both approaches. Moreover, the use of two different paired gel tubes allowed measurement of local variations in the wavelengths. Finally, *in-vivo* experiments with this probe demonstrate the feasibility of detecting natural waves along the esophagus. This study represents the first successful step toward local characterization of the stiffness of the esophagus using natural waves.

2. Materials and Methods

2.1 Preparation of polyvinyl alcohol gels

To model the esophagus, two polyvinyl alcohol gel tubes of different elasticities were made. The gels were prepared as described in [26] and [27] but without the initial strain since we did not need our gel to be anisotropic. The soft gel tube (here referred to as the S-gel tube) contained 10% polyvinyl alcohol (Poly(vinyl alcohol) 99+% hydrolysed, Mw85,000-124,000. Sigma-Aldrich, USA) and underwent two freezing cycles, while the hard gel (H-gel) tube contained 10% polyvinyl alcohol and underwent three freezing cycles. Graphite particles (Graphite powder MW12.01 Fischer Scientific, UK) were added at <1% to both preparations to provide a darker color to improve the contrast with the background for the camera. A cylindrical mold was used to provide the cylindrical shape similar to the esophagus. The mold was a 13 mm diameter, 250 mm long tube with a removable 10 mm diameter rod inside.

2.2 Experimental set-up

Figure 1 shows the experimental set-up. This comprises the gel tube on the light table with a vibrator on each side positioned at the entrance of the gel tube, with the luminal probe (Endoflip™; Medtronic, Minneapolis, MN, USA) inserted into the gel tube. We use two vibrators to generate symmetrical waves in the tubes. The vibrators are synchronized and deliver 5 s sweeps from 5 Hz to 20 Hz. These frequencies were chosen because they fit the order of magnitude of the usual frequency range for natural[28]. As explained in the result section, it appeared that non linearities in the vibrators caused emission of frequencies up to 60Hz (third harmonic of the emitted frequencies). The vibrators are powered by an amplifier, to amplify the signals delivered by the generator. The field of view of the camera (Chronos 1.4; Kron Technologies Inc., Burnaby, BC, Canada) that is positioned vertically above the set-up includes the gel tube and the vibrators (Fig. 1b). The gel tube is positioned along a light box. The camera is held above the table by a mechanical arm, while the probe is inserted into the gel tube. The two synchronized vibrators (APA600MML; Cedrat Technologies, Meylan, France) are positioned on each side of the gel tube at the level of the upper part of the gel tube. The camera takes exposures at 1000 frames per second at 180 μm resolution. The probe records 10 measures per second, and with the impedance sensors separated by 5 mm, this provides unidimensional spatial resolution of 5 mm. The balloon of the probe is filled with 20 mL saline solution to ensure good contact between the balloon and the gel tube. Three series of acquisitions were made using various combinations of paired S-gel and H-gel tubes: two S-gel (S–S-gel) tubes, two H-gel (H–H-gel) tubes, and the combination of one S-gel tube and one H-gel tube (S–H-gel tube). Coupling of the gels was ensured by overlapping them, thrusting one tube in the other. In the two first cases, two gel tubes of the same stiffness were used instead of one longer gel tube, to control for the effects of the overlapping interface along the tube. The source position impact was also studied. The data were processed for the upper part (i.e., near the excitation sources; Figure 1, left) of the S–S-gels (S–S near), the lower part of the S–S-gels (S–S far; Figure 1, right), the S–S-gel tubes as a whole (S–S-whole), the corresponding parts of the H–H gel tubes (H–H near, H–H far, H–H whole), the soft part of the S–H-gel tubes (S–H soft; ‘upper’ end near the vibrators) and the hard part of the S–H-gel tubes (S–H hard; distant end from the vibrators).

Gel pair	Overlap	size of gel near	size of gel far	Wall thickness	Inner diameter
S-S	10	70	90	3	3
S-H	10	70	60	3	3
H-H	10	60	80	3	3

***Table 1**: Gel tubes dimensions expressed in mm*

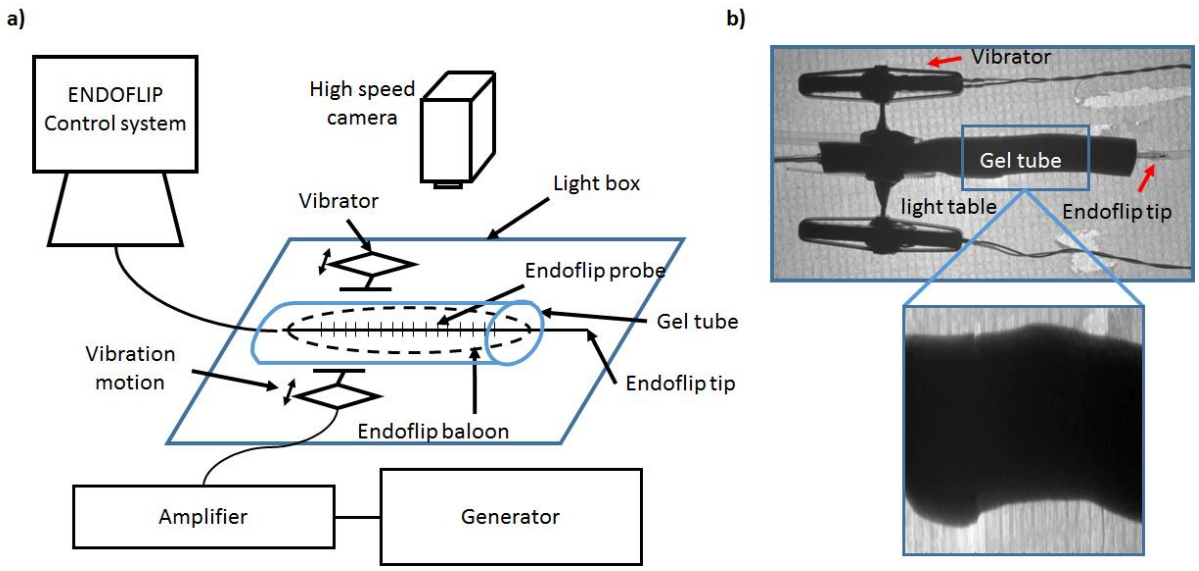

Figure 1. *(**a**) Experimental set-up. A high speed camera positioned above the set-up images the gel tube with the probe in its saline balloon positioned inside the gel tube on a light box. Elastic waves are generated using the pair of vibrators, positioned either side of the gel tube, at the 'upper' end. (**b**) Typical view from the camera, and example of a selected magnified image used for the analysis.*

2.3 Data processing for the camera

To avoid electronic and optical noise, the spectrum of the time series of each pixel of the movies was computed and then a low-pass filter based on the frequency for the still background of the image was applied. The background of the image behind the gel tubes is not supposed to move therefore we assume that all the signal changes in the pixels of the background can be considered as noise. By computing the spectrum of the signal in those pixels we hope to get the high frequencies of the noise which we believe to be mostly optical and due to the camera acquisition. The right and left edges of the gel tubes were segmented using simple thresholding of the intensity of the gray levels in each image of the movie. Those contours can be seen in Figure 2a, highlighted in blue for the left edge and in red for the right edge. The difference in the section of the gel tube at the top of the image in Figure 2 is due to the imbrication of two different gel tubes, which allowed the interface between the two gel tubes to be seen. A phase tracking algorithm was then used on the imaginary part of the Hilbert transform of the movie, to obtain the displacement field at every pixel of every frame [29]. The displacement was then spatially smoothed for each frame using a median filter of 15 by 15 pixels. A directional filter was then applied to cancel the wave reflections going from bottom to top. This directional filter was applied by computing the two-dimensional Fourier transform along the horizontal axis and the time for each height, with all of the values of the upper left quadrant and lower right quadrant in the frequency domain set to zero. Thus, all motion going from the bottom to the top was cancelled. Since we are applying this filter in only one direction and one dimension, its implementation is simple and does not introduce artifacts. Figure 2b shows a frame of the displacement movie on which the edges of the gel tube and the arrows that indicate the direction of the movement of these edges are superimposed. The movements observed inside the gel tube might be due to lighting changes on the surface caused by the movement of the gel tube. It can also be seen that symmetric and antisymmetric wave propagation modes coexist in the gel tube.

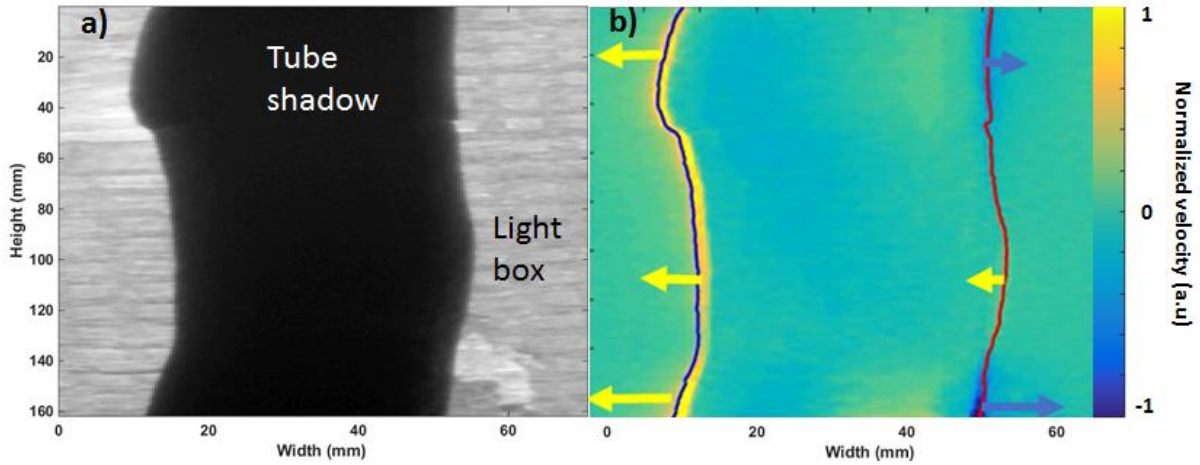

Figure 2. *(**a**) Photograph of the soft–soft (S–S)-gel tube. The highlighted contours in blue and red are also shown in (b). (**b**) Particle velocity field. The blue indicates righthand-side motion, and the yellow indicates lefthand-side motion, as indicated by the arrows.*

To compute the diameter variations along the gel tubes, the displacement of the pixels of the right edge was subtracted from the displacement of the pixels of the left edge of the gel tubes. Wave propagation of symmetric modes was the only specific aspect included in the scope of the present study. This choice was a direct consequence of the way in which this probe works: it only measures the diameter of the gel tubes at different locations. A whitening process was applied to maximize the weight of all of the frequencies where the amplitude was above the amplitude of the frequency of the optical noise computed previously. This whitening process was made by inverse filtering: all frequencies for which the amplitude was below the threshold defined above were set to one in the Fourier domain before transforming back to temporal domain. The goal was to rebalance the frequency content of the signal. The measurements along the gel tubes at every frame allowed the axisymmetric wave propagation to be tracked. Figure 3 shows a set of typical signals of the diameter velocity using the camera, and of the diameter using the probe. Here we can see that the delays between peaks is varying. This can be explained by the dispersivity of the medium. As we are following a group of waves of various frequencies it is expected that the phase lag will not remain constant along the tube.

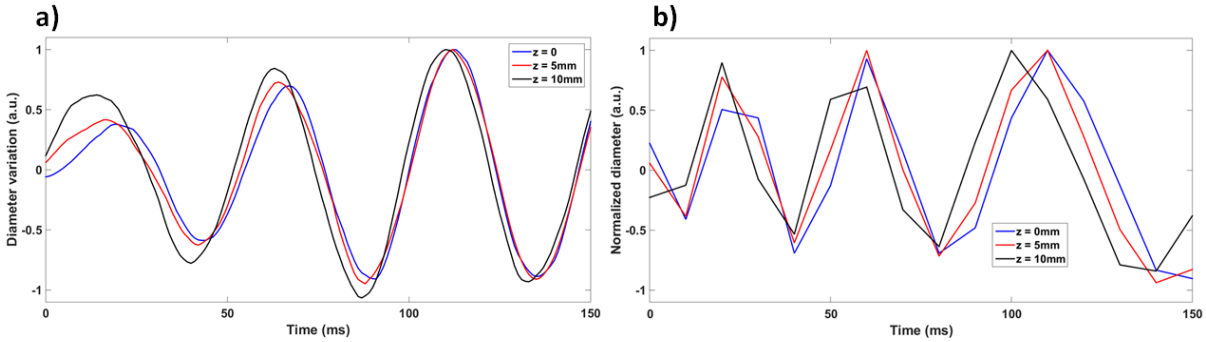

Figure 3. *(**a**) Diameter velocity of a gel tube obtained from the camera at three different positions from the source, as z = 0, 5 and 10 mm. The similarity of the signals and the lag between the peaks indicates the propagation of waves. (**b**) Diameter of the gel tube obtained from the probe at three different positions from the source, as z = 0, 5 and 10 mm.*

Once the field is measured as function of space (Fig. 3), the next step in passive elastography is to compute the correlation between the signals. As an illustration, the field measured in the present experiment was the difference of the particular velocities of the edges which we will call diameter variation. It was measured point by point along the gel tubes. The correlation matrices of Figure 4 have to be interpreted as follows: the first point of the

first matrix row corresponds to the normalized correlation coefficient obtained from the very first measuring point with itself. Thus, the autocorrelation gives unity. Then the correlation coefficient between the field of the first and the second point gives the second point of the first row. This cross-correlation is smaller because the field is slightly different: it starts to lose its coherence. This continues to decrease with the following points. Finally, the first row gives the spatial coherence when the signal of point #1 is taken as a reference. In the second row, the signal of point #2 is taken as the reference, and so on. The correlation coefficients obtained are organized into the correlation matrix. This is a symmetric matrix because the correlation operator is symmetric and its size is the number of pixel in the vertical dimension. The diagonal of the matrix represents the normalized correlation of each reference signal with itself. This matrix was averaged along the diagonal before and after the interfaces between the different gel tubes. This average was computed according to the following equation for every k with m+k in range [1;n]

$$P_{m+k} = \frac{1}{n+k} \sum_{i=1}^{n-k} C_{i,i+k}$$

Equation 1

Here, n is the size of the correlation matrix, m is the index of the maximum correlation worth n/2 or (n+1)/2 depending if n is odd or even, C are the coefficients of the correlation matrix. This equation gives us a linearly distributed weighted average where the maximum correlation is averaged on n points whereas the extreme points are computed according to a single point.

The standard deviation computed to evaluate wavelength dispersion is weighted the same way.

The way the averaged correlation field decreases is related to the wavelength. This whole curve is called the focal spot (Figure 4c, d). Indeed, from a physical point of view, the correlation is equivalent to time reversal, and the zero-lag time gives the focal spot [27]. As a consequence, the -6 dB width gives an estimation of half the mean wavelength of the section of gel tube studied. Due to the smoothing filter used to reduce noise on the data, correlation of displacement at close heights are artificially increased. This induces a peak of highly correlated values that has no physical meaning. Its width is the size of the kernel of the smoothing filter. Therefore we decided to approximate the actual focal spot by truncating 15 values on each side around the maximum of correlation. It is worth noting that the sampling frequency of the data obtained with the high-speed camera would allow the wave speed to be computed. However, due to the time resolution of the probe (~10 Hz), the frequency content of the wavefield cannot be measured with this device, and therefore only the wavelength estimates are presented here.

2.4 Data processing for the probe

Due to the relatively poor sampling in space and time, no filters were applied to the data gathered with the probe. Also, the probe measured the diameter along the gel tubes directly, and therefore these raw data were used to compute the correlation matrix and focal spot profile as given above for the camera data. However focal spots were not truncated since no filter was applied. Considering the low number of points we had for the focal spots, the weighted average focal spot and the weighted standard deviation of these average focal spots are to be considered with care.

2.5 Shear Wave Elastography measurements

In order to have a completely different measurement method, we used the Aixplorer (SuperSonicImagine, France) to measure Youngs modulus in the gels. Gels were immersed in a water tank laying on an absorbent material. The wave length is derived from Young's modulus with the following equation.

$$\lambda = \alpha\, c_R = c\frac{\sqrt{\mu/}}{f} = \alpha\,\frac{\sqrt{(E/3\rho)}}{f}$$

Equation 2

Where λ is the wavelength, E is Young's modulus, c_R is the Rayleigh wave velocity, ρ the material density which is assumed to be 1000kg/m^3 for our tubes, f the central frequency and c the dispersion coefficient. This dispersion coefficient is linked to the frequency regime. At low frequencies, L(0,1) mode waves can be assumed to be symmetric lamb waves [19] and their velocity is the double of the Rayleigh wave velocity hence α =2. At high frequencies, their velocity is the Rayleigh wave velocity hence α is =1. Therefore, knowing the frequency content of the wave field, we can use these measurements to give a range of possible wavelengths in the gel tubes.

2.6 In vivo measurements

We used a set of data gathered during a clinical examination. The examination with the luminal probe was part of the routine examination for a patient with dysphagia and suspicion of esophageal motility disorder unproven with other testings. The subject was a 66 year old man. Luminal probe measurements were performed after an upper gastro-intestinal endoscopy in the sedated patient. Propofol and remifentanil were used for the sedation. The probe was inserted within the esophagus, positioned on the esophago-gastric junction and the balloon of the probe was filled with 40ml of saline solution.

Informed consent to use these data for research purpose after anonymization was given by the patient. According to French law, this type of analysis of data, obtained during the clinical evaluation of patients, does not require ethical board review.

3. Results and Discussion

3.1 Camera and probe

A focus on the data obtained with the combination of two equally soft (S–S) gel tubes is used here to illustrate the data for both of these imaging modalities.

Figure 4a shows the correlation matrix obtained with the camera data, with the interface between the S–S-gel tubes at the height of pixel 150. This appears to affect the correlation pattern only locally, with a minor interface effect seen on the propagation of the waves. The correlation matrix shows a homogeneous pattern along the gel tubes, which allows the correlations along the diagonal of the matrix to be averaged to obtain the focal spot profile in Figure 4c. As explained in the previous section, top values were truncated, and the focal spot was normalized to the new maximum. Half the wavelength is given by the width at a correlation of 0.5. Here the pixel size is 180 μm, thus giving a wavelength of 35.8 mm.

Although the correlation matrix of the probe data in Figure 4b is not as homogeneous as with the camera, a pattern along the diagonal can still be seen that provides enough information to compute the wavelength. However, the junction between the gels at the eighth sensor is more prominent than seen for the camera, and the last two sensors show a widening of the correlation pattern. The wavelength obtained here is 38 mm. The correlations are globally higher with the probe. This might be due to electronic drift in the measurements from the probe, as such drift is common to all sensors, whereby the correlation is globally increased.

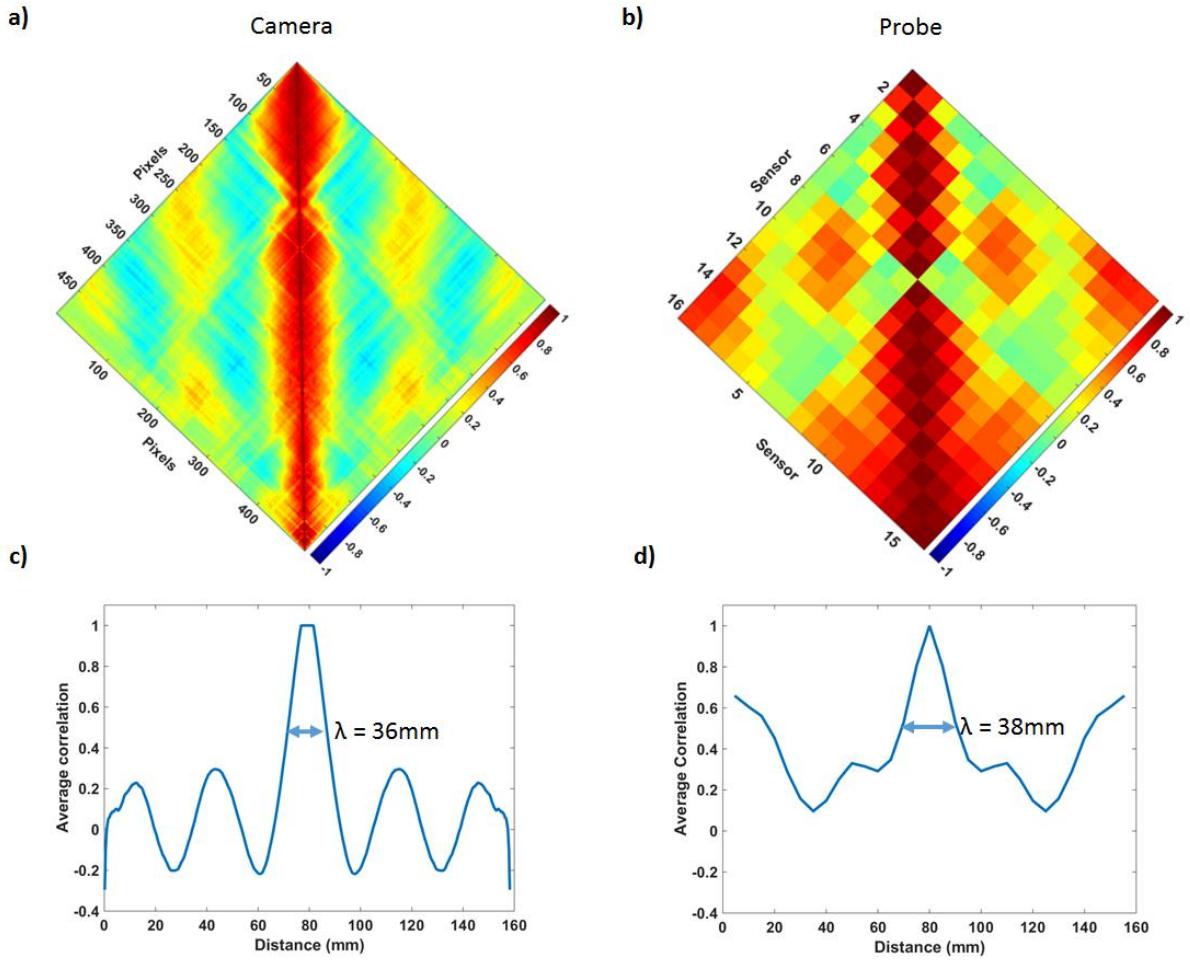

Figure 4. *(**a, b**) Correlation matrices obtained with the camera (a) and the probe (b) for the S–S-gel tubes. Red indicates high correlation. They have been rotated by 45° to give better understanding of the averages below. (**a**) For the camera, as expected, the pixels close to each other are highly correlated along the central line, with a pattern of alternating high and low correlation away from the central line. The interface between the gel tubes is at pixel 150. (**b**) For the probe, the smaller size of the domain studied allows only the beginning of the correlation pattern observed with the camera to be seen. The interface between the gel tubes is at sensor 8. (**c, d**) Averages of the correlation matrices along the matrices diagonals (vertical line on the rotated matrices) for the camera (c) and the probe (d), with wavelength measures indicated.*

The camera data allowed all of the focal spots of the different gel combinations to be computed. These were not noisy, with clear wavelength measures obtained. As expected, the central peak of these focal spots was wider for the H-gel tubes (see Supplementary Figure S1). Differences were seen between the S-gel and H-gel tubes, whereby the central peaks were wider for the H-gel tube. The S–S far measures were the only exception here, which showed a central peak as wide as S–H hard. The same calculations with the probe data provided equivalent focal spots (See Supplementary Figure S2), where it was possible to discriminate between the S-gel tube and the H-gel tube.

The results of the wavelength calculations based on these average focal spots are summarized in Figure 5. Apart from S–S far, there was an excellent match between the camera and probe acquisitions, with consistent data obtained for the S-gel tube and the H-gel tube for every acquisition. The average wavelengths across all of the acquisitions were 37 mm (standard deviation, 6 mm) for the S-gel tube, and 61 mm (standard deviation, 9 mm) for the H-gel tube. A large part of the variability of the measurements for the H-gel tube was due to S–H hard.

Although the S–H hard wavelength was greater than that for the S-gel tube, this wavelength is surprisingly low for both imaging modalities. The interface between the S-gel and H-gel tubes might have been responsible for this phenomenon, considering that to ensure the stability of the gel tubes under vibration, the H-gel tube was slightly overlapping the S-gel tube, and it is possible that the S-gel tube imposed its own vibrations onto the H-gel tube close to the interface. It is also important to remind here that the error on each measurement is the weighted standard deviation defined in the method section. The low number of measure points for the probe focal spots increases drastically the importance of the interface on the error bars as can be seen on figure 4 b).

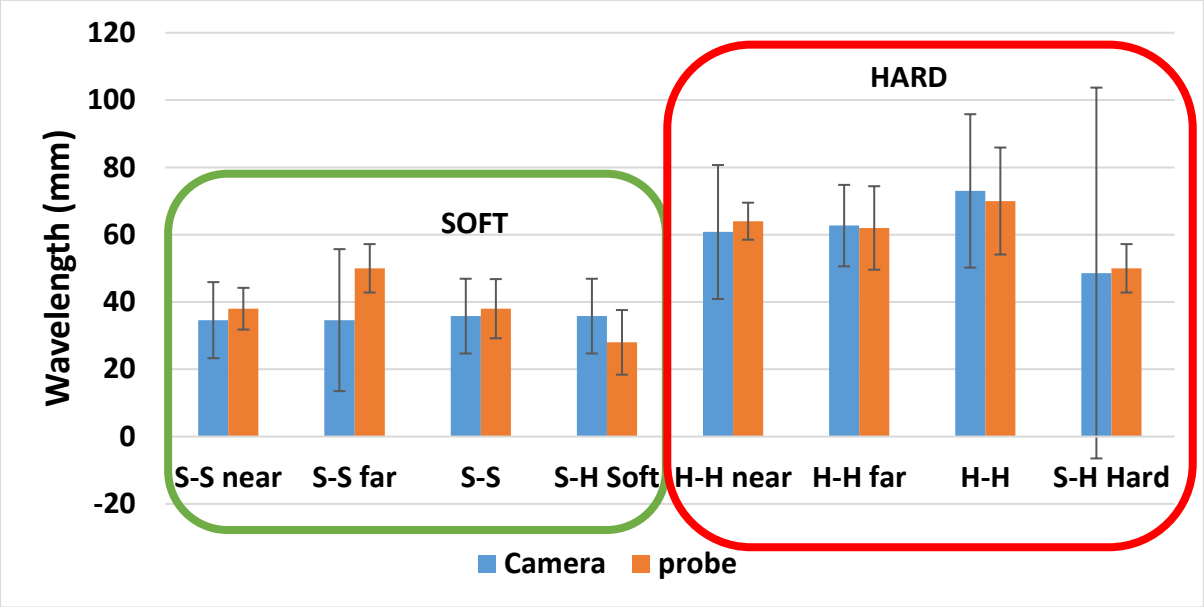

Figure 5. *Wavelengths obtained with the two imaging modalities for the different gel tube combinations. For gel tube abbreviations, see main text.*

3.2 Shear wave elastography

The Young's modulus measurements gave us 25 kPa for the gel H and 8 kPa for gel S. The central frequencies measured in the gels are 41 Hz for gel S and 67 Hz for gel H. This gives us wavelength ranging from 4 mm to 9 mm for gel H and 4 to 8 mm for gel S which is in good accordance with the camera and probe measurements. These frequencies are higher than those of the excitation source. This can be explained by non linearities from the vibrators occurring when vibrating at high amplitude and between each sweep cycle. Even if those frequencies may end up not being as physiologically relevant as the ones of the excitation source, the wavelength values still validate camera and probe measurements.

We have shown here that two different imaging modalities can be used to compute wavelengths in gel tubes and can accurately discriminate an S-gel tube from an H-gel tube. Despite the relatively poor resolution of the probe, relevant data was obtained that allowed computation of the wavelengths, with values that are consistent with those for the high-speed camera. However, the lack of precision with the probe, whereby well-resolved images are not obtained, is currently of concern, due to the low spatial resolution. The effects seen at the interface between the S-gel tube and the H-gel tube also indicate that where several different elasticities need to be explored on a small

scale, this probe might not discriminate between them. However, this issue should be easily resolved by increasing the number of sensors on the probe. Furthermore, the increased acquisition frequency would also allow wave speeds to be computed, in addition to wavelengths.

3.3 In Vivo experiment

It is also important to note here that the level of vibrations used in these experiments might not be perfectly representative of the actual physiological movements that will allow fully passive elastography. In other words, does this probe allow for In Vivo wave length measurements? To obtain more insight into this, we tried our algorithms on *in-vivo* data collected on a patient who was undergoing a clinical examination. Here, we were not able to compare these data with camera data, and also, as the actual clinical examination was aimed at measuring the distensibility of the esophago-gastric junction, only seven probe sensors were introduced into the esophagus. However, the pattern obtained for the correlation matrix gives us hope that it will be possible to perform *in-vivo* passive elastography of the esophagus using the luminal probe as it is, or potentially with minor electronic modifications. The correlation matrix and average focal spot shown in Figure 6 are characteristic of a well-defined wavelength. The low number of sensors in the esophagus prevented any definitive value to be assigned to this wavelength, as the focal spot profile is limited in range. However, these data provide the first rough estimate of the average wavelength of this esophagus, as 50 mm.

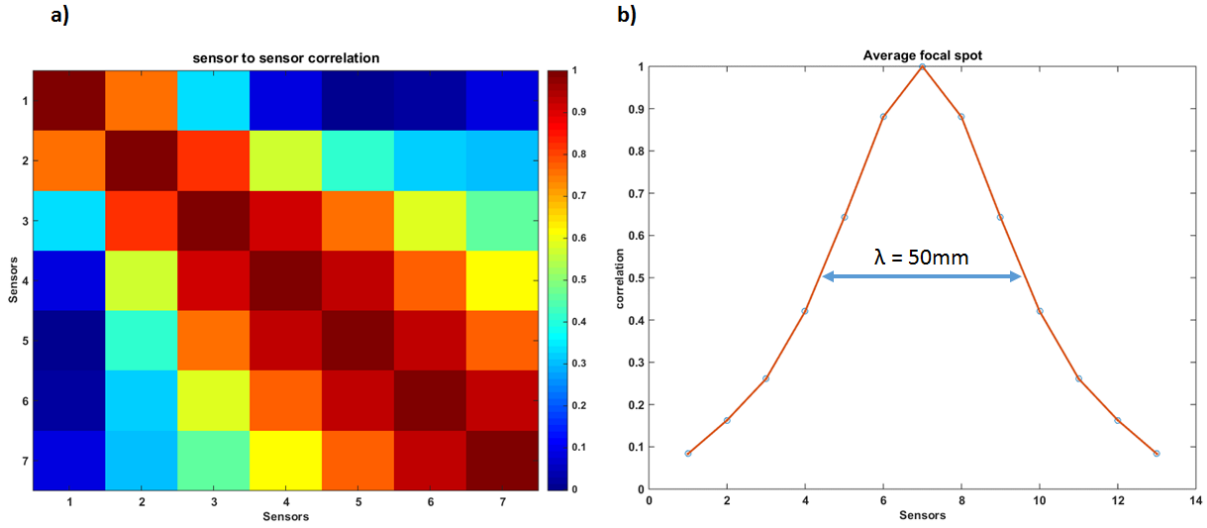

Figure 6. In-vivo *data obtained with the probe, for the correlation matrix (**a**) and the average focal spot (**b**).*

Assuming a central frequency range of 20Hz for natural waves [28], equation 2 gives a shear modulus ranging between 0.75kPa and 3kPa, These values seem plausible when compared to porcine ex vivo values in [25] (around 10kPa) as we expect living tissues to be softer than dead tissues. However, the frequency content of the waves propagating in the esophagus can not be known with the probe because of its low sampling frequency, therefore we cannot be sure neither of the central frequency nor of the frequency regime. We assume that further experiments based on a protocol dedicated to wavelength assessment, and that would include all of the sensors in the esophagus, will allow determination of the wavelength with more confidence and precision.

Even if it is possible to reach a statistically significant number of samples to obtain a robust value for the wavelength of the human esophagus, a major issue here is the lack of a 'ground truth' for this measurement, as it has not been obtained to date by any other means. As mentioned, we think that precise quantitative *Ex-vivo* analysis cannot be considered here, because the *ex-vivo* esophagus will certainly not have the same mechanical properties as the living human tissue.

One option would be the use of the same methodology with a different imaging modality to measure the wavelength. Magnetic resonance imaging is not fast enough, as its time resolution can hardly exceed 2 Hz, and echography is limited because the trachea masks the esophagus. We believe that ultra-fast X-ray tomography might instead meet these challenges. However, as this method gives a projection of all of the planes, the transparency of all of the tissues might be an issue. However, as with the use of camera here we are only considering the propagation of waves in two dimensions, in terms of the cylindrical geometry of the gel tubes, we might be able to track only the most external parts of all of the projected planes in a human esophagus with an X-ray device. This would probably provide access to the propagation of symmetric modes in the esophagus *in vivo*. Moreover, if X-rays can indeed be shown to be relevant, this method could be applied to any other tube-shaped structure in the human body, such as the trachea and bowels, and potentially even the arteries.

4. Conclusion

Here, we have carried out a first study to assess the feasibility of using the propagation of waves to quantify the elasticity of soft tube walls. By this comparison of two different imaging modalities, we were able to measure the wavelengths in gel tubes that mimic the human esophagus. As one of these modalities is a medical device that is already used in common clinical practice (i.e., the probe), this system is of great interest as it would only need minor adjustments to be used for this new purpose in the human body. We also showed differences between tubes made from soft and hard gels paired with one another. We thus believe that it will be possible to measure local differences in wavelengths in tube-shaped organs. These wavelengths are directly related to the elasticity of the soft materials. They can be used as biomarkers to characterize the esophagus, as the stiffness of this organ appears to have a major role in several pathologies. The consistency of the data here gives us confidence of the potential of this technique and its application. However, to be fully efficient, this method needs several adjustments and verification, as we cannot state with certainty that the natural waves in the human body provide enough information. However, our first set of *in-vivo* data indicates that it is possible to obtain the relevant measurement. These measurements now need to be repeated with a protocol dedicated to wave tracking. We also need to find a way to challenge these data through other methods, as there is currently no ground truth regarding wavelengths in the esophagus *in-vivo*.

Acknowledgements

This work was funded by ARC 2015 of PhysiCancer. We aknowledge John O'Dea and Crospon for technical support.

[1] F. Zerbib et T. Omari, « Oesophageal dysphagia: manifestations and diagnosis », Nat Rev Gastroenterol Hepatol, vol. 12, no 6, p. 322-331, juin 2015, doi: 10.1038/nrgastro.2014.195.

[2] H. Gregersen, « Analysis of Functional Luminal Imaging Probe Data », Clinical Gastroenterology and Hepatology, vol. 15, no 8, p. 1313-1314, août 2017, doi: 10.1016/j.cgh.2017.04.010.

[3] L. Sandrin et al., « Transient elastography: a new noninvasive method for assessment of hepatic fibrosis », Ultrasound in Medicine & Biology, vol. 29, no 12, p. 1705-1713, déc. 2003, doi: 10.1016/j.ultrasmedbio.2003.07.001.

[4] S. Catheline, F. Wu, et M. Fink, « A solution to diffraction biases in sonoelasticity: The acoustic impulse technique », The Journal of the Acoustical Society of America, vol. 105, no 5, p. 2941-2950, mai 1999, doi: 10.1121/1.426907.

[6] A. Zorgani et al., « Brain palpation from physiological vibrations using MRI », Proc Natl Acad Sci U S A, vol. 112, no 42, p. 12917-12921, oct. 2015, doi: 10.1073/pnas.1509895112.

[7] T.-M. Nguyen, A. Zorgani, M. Lescanne, C. Boccara, M. Fink, et S. Catheline, « Diffuse shear wave imaging: toward passive elastography using low-frame rate spectral-domain optical coherence tomography », J Biomed Opt, vol. 21, no 12, p. 126013, déc. 2016, doi: 10.1117/1.JBO.21.12.126013.

[8] R. Muthupillai, D. Lomas, P. Rossman, J. Greenleaf, A. Manduca, et R. Ehman, « Magnetic resonance elastography by direct visualization of propagating acoustic strain waves », Science, vol. 269, no 5232, p. 1854-1857, sept. 1995, doi: 10.1126/science.7569924.

[9] R. S. Sahebjavaher et al., « MR elastography of prostate cancer: quantitative comparison with histopathology and repeatability of methods: TRANSPERINEAL PROSTATE MRE: INITIAL PATIENT STUDY », NMR in Biomedicine, p. n/a-n/a, nov. 2014, doi: 10.1002/nbm.3218.

[10] F. Dittmann, S. Hirsch, H. Tzschätzsch, J. Guo, J. Braun, et I. Sack, « In vivo wideband multifrequency MR elastography of the human brain and liver: In Vivo Multifrequency wMRE of the Human Brain and Liver », Magn. Reson. Med., vol. 76, no 4, p. 1116-1126, oct. 2016, doi: 10.1002/mrm.26006.

[11] A. Ramier, B. Tavakol, et S.-H. Yun, « Measuring mechanical wave speed, dispersion, and viscoelastic modulus of the cornea using optical coherence elastography », Optics Express, vol. 27, no 12, p. 16635, juin 2019, doi: 10.1364/OE.27.016635.

[12] A. Nahas, M. Tanter, T.-M. Nguyen, J.-M. Chassot, M. Fink, et A. Claude Boccara, « From supersonic shear wave imaging to full-field optical coherence shear wave elastography », Journal of Biomedical Optics, vol. 18, no 12, p. 121514, déc. 2013, doi: 10.1117/1.JBO.18.12.121514.

[13] J. J. Pitre et al., « Nearly-incompressible transverse isotropy (NITI) of cornea elasticity: model and experiments with acoustic micro-tapping OCE », Sci Rep, vol. 10, no 1, p. 12983, déc. 2020, doi: 10.1038/s41598-020-69909-9.

[14] A. Zorgani, T. A. Ghafour, M. Lescanne, S. Catheline, et A. Bel-Brunon, « Optical elastography: tracking surface waves with digital image correlation », Phys Med Biol, vol. 64, no 5, p. 055007, févr. 2019, doi: 10.1088/1361-6560/ab0141.

[15] S. Catheline, R. Souchon, M. Rupin, J. Brum, A. H. Dinh, et J.-Y. Chapelon, « Tomography from diffuse waves: Passive shear wave imaging using low frame rate scanners », Applied Physics Letters, vol. 103, no 1, p. 014101, juill. 2013, doi: 10.1063/1.4812515.

[16] D. C. Gazis, « Three-Dimensional Investigation of the Propagation of Waves in Hollow Circular Cylinders. I. Analytical Foundation », p. 7.

[17] D. C. Gazis, « Three-Dimensional Investigation of the Propagation of Waves in Hollow Circular Cylinders. II. Numerical Results », The Journal of the Acoustical Society of America, vol. 31, no 5, p. 573-578, mai 1959, doi: 10.1121/1.1907754.

[18] J. Li et J. L. Rose, « Natural beam focusing of non-axisymmetric guided waves in large-diameter pipes », Ultrasonics, vol. 44, no 1, p. 35-45, janv. 2006, doi: 10.1016/j.ultras.2005.07.002.

[19] H. Nishino, S. Takashina, F. Uchida, M. Takemoto, et K. Ono, « Modal Analysis of Hollow Cylindrical Guided Waves and Applications », Jpn. J. Appl. Phys., vol. 40, no Part 1, No. 1, p. 364-370, janv. 2001, doi: 10.1143/JJAP.40.364.

[20] M. Couade, « Ultrafast imaging of the arterial pulse wave », p. 3, 2011.

[21] L. Marais et al., « Arterial Stiffness Assessment by Shear Wave Elastography and Ultrafast Pulse Wave Imaging: Comparison with Reference Techniques in Normotensives and Hypertensives », Ultrasound in Medicine & Biology, vol. 45, no 3, p. 758-772, mars 2019, doi: 10.1016/j.ultrasmedbio.2018.10.032.

[22] M. Couade et al., « Quantitative assessment of arterial wall biomechanical properties using shear wave imaging », Ultrasound Med Biol, vol. 36, no 10, p. 1662-1676, oct. 2010, doi: 10.1016/j.ultrasmedbio.2010.07.004.

[23] M. Bernal, I. Nenadic, M. W. Urban, et J. F. Greenleaf, « Material property estimation for tubes and arteries using ultrasound radiation force and analysis of propagating modes », J. Acoust. Soc. Am., vol. 129, no 3, p. 12, 2011.

[24] E. Maksuti, « Arterial Stiffness Estimation by Shear Wave Elastography: Validation in Phantoms with Mechanical Testing », Ultrasound in Medicine and Biology, vol. 42, no 1, p. 14, 2016.

[25] Aho, Johnathon M., Ivan Z. Nenadic, Sara Aristizabal, Dennis A. Wigle, Daniel J. Tschumperlin, and Matthew W. Urban. "Use of shear wave ultrasound vibrometry for detection of simulated esophageal malignancy in ex vivo porcine esophagi." Biomedical physics & engineering express 2, no. 6 (2016): 065002.

[26] Chatelin, S., Bernal, M., Deffieux, T., Papadacci, C., Flaud, P., Nahas, A., Boccara, C., Gennisson, J.-L., Tanter, M., and Pernot, M. (2014). Anisotropic polyvinyl alcohol hydrogel phantom for shear wave elastography in fibrous biological soft tissue: a multimodality characterization. Phys. Med. Biol. 59, 6923.

[27] Millon, L.E., Mohammadi, H. and Wan, W.K. (2006), Anisotropic polyvinyl alcohol hydrogel for cardiovascular applications. J. Biomed. Mater. Res., 79B: 305-311.

[28] T. Gallot, S. Catheline, P. Roux, J. Brum, N. Benech, et C. Negreira, « Passive elastography: shear-wave tomography from physiological-noise correlation in soft tissues », IEEE Trans Ultrason Ferroelectr Freq Control, vol. 58, no 6, p. 1122-1126, 2011

[29] N. Benech, S. Catheline, J. Brum, T. Gallot, et C. Negreira, « 1-D elasticity assessment in soft solids from shear wave correlation: the time-reversal approach », IEEE Trans. Ultrason., Ferroelect., Freq. Contr., vol. 56, no 11, p. 2400-2410, 2009